THE JOURNAL OF PHYSICAL CHEMISTRY B

Article

pubs.acs.org/JPCB

A Resonance Raman Enhancement Mechanism for Axial Vibrational Modes in the Pyridine Adduct of Myoglobin Proximal Cavity Mutant (H93G)

Stefan Franzen,* Derek Brown, and John Gaff

Department of Chemistry, North Carolina State University, Raleigh, North Carolina 27695, United States

B. Delley

Paul-Scherrer-Institut, WHGA/123, CH-5232 Villigen, Switzerland

Supporting Information

ABSTRACT: The proximal cavity mutant of myoglobin consists of a mutation of the proximal histidine to glycine (H93G), which permits exogenous ligands to bind to the heme iron. A non-native pyridine ligand can ligate to the heme to yield a five-coordinate adduct, H93G(Pyr), that cannot be formed freely in solution since the six-coordinate bis-pyridine adduct is more stable than the five-coordinate adduct. We have used resonance Raman spectroscopy in the Soret band region of the heme to study the enhancement of axial vibrations of bound pyridine in the H93G(Pyr) adduct. The observation that the pyridine ring breathing mode (ν_1) and the symmetric ring stretching (ν_3) modes are enhanced under these conditions is explained by a computational approach that shows that coupling of the π-system of the heme with the p-orbitals of the pyridine is analogous to π-backbonding in diatomic ligand adducts of heme proteins. The result has the broader significance that it suggests that the resonance enhancement of pyridine modes could be an important aspect of Raman scattering of pyridine on conducting surfaces such as those studied in surface enhanced Raman scattering experiments.

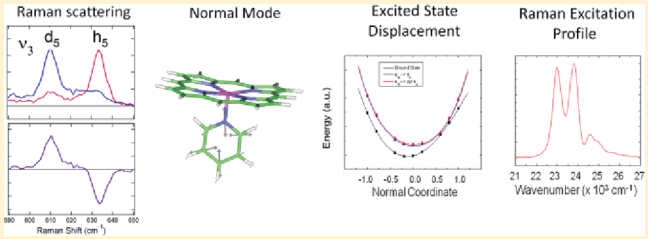

INTRODUCTION

The mechanism of resonance Raman enhancement of axial modes in metalloporphyrins is important to understanding the information they carry concerning axial bonding and the origin of enhancement effects of molecules in metal and surface adducts. The reasons for resonance enhancement of axial ligands can include coupling through bonds to electronic transitions such as the $\pi-\pi^*$ or charge transfer (CT) transitions of the heme. Electronic-nuclear coupling of this type has a relationship to the more general class of resonant enhancement mechanisms for molecules bound to surfaces, although the role played by surface plasmon bands has not often been considered in the context of resonance Raman enhancement. Metalloporphyrins are an interesting case since the intense Soret band has a clearly defined directionality vis-à-vis axial ligands, and the bonding can be dissected readily into σ- and π-type contributions, which permits a more facile analysis of the nature of the effect than in other metal adducts of lower symmetry. For both molecules and surfaces, electronic transitions can couple to molecular vibrations through the chemical bond between the molecule and the surface. For example, surface attached molecules that are enhanced by plasmonic transitions may have a resonance component due simply to the displacement of nuclear coordinates in response to electronic excitation of the surface.[1] This observation and associated calculations have led to the suggestion that resonance the Raman enhancement mechanism is one possible explanation for the large enhancement in surface enhanced Raman scattering (SERS).[1]

Pyridine has been one of the most common molecular substrates used in SERS studies since its discovery in 1974.[2−19] Herein, we consider the analogous effect of excitation of the heme in a plane orthogonal to the molecule vibrations of pyridine bound axially to the heme iron. In heme proteins, an axial amino acid residue acts as the ligand to the heme iron and is the sole covalent connection between the heme and protein in globins and many enzymes. Many resonance Raman studies have shown that axial ligand motions are enhanced by laser excitation in the region of a $\pi-\pi^*$ transition. The observation of the Raman active band in the 180−250 cm^{-1} region ascribed to an iron−ligand (Fe−L) axial out-of-plane mode has been a useful signature of ligand identity and protein conformation state for a range of heme proteins.[20−26] However, π-acid ligands

Special Issue: Richard A. Mathies Festschrift

Received: March 1, 2012
Revised: May 9, 2012
Published: May 25, 2012

such as CO, NO and O_2 also exhibit enhancement of Fe−XO stretching and Fe−X−O bending vibrations as well as of X−O stretching vibrations.[27] By contrast, the resonant effects on σ-donor ligands have been confined to the axial Fe−L stretching vibration, such as the Fe−His and Fe−Cys vibrations in proteins. It has been shown elsewhere that Fe−L σ-donors are enhanced only in five-coordinate heme adducts.[28,29] Traditionally, the observable axial vibrations have been limited by the intrinsic axial ligands of cysteine and histidine, which are the common ligands for such adducts in the repertoire of the naturally occurring amino acids. Given the large number of studies of pyridine on surfaces, it is of interest to consider the resonant effects on pyridine axially ligated to a heme protein. However, since the pyridine moiety is not present in the amino acids, it is necessary to resort to a semisynthetic approach to generate such a model.

We consider a model system that permits construction of a five-coordinate adduct to test for resonant effects on axial ligation. The H93G proximal cavity mutant of Sperm whale myoglobin (SWMb) can be prepared with a series of ligands L in the proximal cavity, H93G(L) to provide a versatile model system for the study of five-coordinate heme adducts.[30−35] Studies of five-coordinate H93G(L) adducts can be used to probe effects on ligand rebinding rates, spectroscopic properties, structure, and thermodynamic stability of ligand binding. Although resonance Raman spectra axial modes in a six-coordinate bis-pyridine iron(II) heme complex have been observed,[18] the enhancement at ∼490 nm was assigned a resonance with a CT band. This CT π-coupling is distinct from coupling to the Soret band itself, which can be either of σ- or π-type. The calculations suggest that there are CT bands buried under the Soret band, although these have much lower intensity. Of interest here is the analogy between coupling of the pyridine ligand to the heme, which has similarity to the coupling of pyridine molecules to metal surfaces, including metals such as Ag, Co, Ni, and Fe.[36] In the coupling of molecules to metal surfaces, there is a long-standing suggestion that CT transitions play a role in Raman enhancement. In this study, we develop the analogy of resonant coupling to strongly allowed bands with large oscillator strength as distinct from CT coupling. The significance of resonance Raman enhancement can be understood mainly by the Franck−Condon coupling to a strongly allowed transition, the $\pi-\pi^*$ transition known as the Soret band in metalloporphyrins. Coupling by σ-bonding from the nitrogen (N_ε) lone pair to the heme Fe is a well-established electronic coupling in bound histidine that can to lead to enhancement of axial modes in a five-coordinate complex, although the only enhanced modes that have been observed are the Fe−N_ε or Fe−His stretching vibrations and not internal ring modes of the imidazole ring of histidine.[28] There have been no reports of enhancement of bis-imidazole in six-coodinate adducts, although pyridine and N-methyl imidazole axial modes have been observed to be enhanced in axially asymmetric complexes with Fe metalloporphyrins.[37] However, the analogy with a surface is best made in a five-coordinate metalloporphyrins adduct. Attempts to prepare a five coordinate pyridine metalloporphyrin fail in solution because the formation of the bis-pyridine complex is much more favorable than the monopyridine complex. The protein-based H93G model system has permitted the preparation of a five-coordinate heme−pyridine complex.[31,35,38,39]

We can compare experiment to theory using a calculation of the excited state displacements as a method for estimating the intensity of resonance Raman active modes. In this study we have used a method for the calculation of Raman excitation profiles (REPs) developed by Shreve and Mathies based on an application of the time-correlator formalism that includes thermalized modes, such as the axial modes of heme proteins.[40] While there are factors such as the excited state dephasing rate and transition moment that determine the absolute resonance Raman cross sections, the excited state displacements determine the relative intensities, which is our main interest here in assessing whether the modes observed in Raman spectra are enhanced by a resonant Raman mechanism. In a weak coupling Franck−Condon model for resonance Raman enhancement, the intensity of a Raman band is proportional to the displacement along a given normal mode coordinate in the excited state. As the molecule departs from the ground state equilibrium geometry, via the coordinate Q, the transition moment is altered.[41] The expression for the polarizabilty that describes this mechanism consists of two terms, called A and B, which represent scattering by Franck−Condon and Herzberg−Teller mechanisms, respectively. The time-correlator formalism for the calculation of resonant Raman cross sections rigorously applies only to A-term enhancement, which involves totally symmetric modes. REPs have demonstrated that iron−histidine mode in myoglobin is enhanced predominately by an A-term scattering mechanism. This is also evident from the polarized nature of the mode. REPs have shown that the vibronic component of the out-of-plane axial ligand stretching mode is relatively small.[42] The Raman bands from iron−pyridine out-of-plane motions and pyridine ligand modes are also polarized. The enhancement of these modes by an A-term scattering mechanism implies that there must be a displacement along these normal-mode coordinates in the excited state. Enhancement mechanisms for in-plane modes of metalloporphyrins have been explained by both mechanisms since there are important totally symmetric modes such as ν_3 and ν_4 in the Raman spectrum. However, vibronic coupling is also important in hemes, and non-totally symmetric modes such as the core-size marker modes, ν_{10} and ν_{11}, are also important in Raman scattering in resonance with the heme Soret band.[43−45] While modes are important for vibronic coupling of the formally forbidden Q-bands and CT bands,[46] they do not participate in enhancement of axial vibrations, which are of interest here.

The largest SERS enhancements for internal modes of pyridine on Ag are observed for totally symmetric pyridine ring vibrations,[6,14,47] which may provide evidence to support the contention that the Albrecht A term polarizability makes the largest contribution to the SERS scattering.[1] The view that the Herzberg−Teller or B-term enhancement is important has been advanced as well.[48] B-term scattering is a different mechanism that does not involve excited state displacements, but rather involves the coupling of higher lying states by means of distortions of the symmetry. This point has not been fully considered in the theory of SERS, and it is of interest to understand which mechanism is operative. Heme is an especially interesting molecule for comparison to surfaces since the role played by A-term and B-term, (i.e., Franck−Condon and Herzberg−Teller couplings) are distinguished by the REPs of various modes.[42,46,49] The experimental observations and calculations in this study suggest that there is a similar Franck−Condon coupling between pyridine on Ag and pyridine ligated to heme. This type of comparison has precedent in a number of Ag adducts that have been studied previously in order to explain the variability of Raman

frequencies on Ag surfaces.[36,50] These studies justify the use of a well-defined molecular structure to understand Raman enhancement of modes in pyridine that are also observed in SERS spectra.

EXPERIMENTAL SECTION

In this study, we dialyzed pyridine and d^5-pyridine into the proximal cavity of SWMb, known as H93G, and obtained the five-coordinate deoxy resonance Raman spectra for each complex using Raman excitation ranging from 424 to 452 nm. Samples of H93G SWMb with pyridine and d^5-pyridine were prepared by dialysis as discussed previously.[33,35,51] The samples were prepared in 10 mM pH 7 phosphate buffer. The deoxy form of H93G was prepared by dilution into deoxygenated buffer followed by reduction with excess dithionite. Solutions were placed in a NMR tube spinning cell at ambient temperature. Resonance Raman spectra were obtained by exciting the Soret band of five-coordinate deoxy H93G-pyridine at 424−452 nm using a Coherent 700 dye laser operated with Stilbene 420 dye and pumped with the tripled output of a mode-locked Antares 76-YAG laser (Coherent). The Raman data was calibrated using toluene, cyclohexane, carbon tetrachloride standards, and lines from the atomic emission spectrum of Kr and Ar lamps. Beams from the laser were collimated and cylindrically focused to a vertical line of 0.5 mm, and typically 20−35 mW of laser power was employed at the sample. Raman scattered light was passed through a Spex 1877 Triplemate monochromator and was detected by a liquid N_2-cooled charge-coupled device (CCD) camera (ISA Spex, model CCD-3000). Samples were injected into sealed, N_2-purged NMR tubes and spun with an air piston spinning sample holder (Princeton Photonics, model Raman 101). Spectra were measured at room temperature for three acquisitions with exposure times of 20−120 s, alternating between H93G(d^5-pyr) and H93G(pyr) to minimize sample degradation. In samples where an internal standard was used, 0.2 M Na_2SO_4 was added to the solution. The intensities of the Raman bands were determined relative to the 984 cm^{-1} band of the sulfate standard.

A normal coordinate analysis of the internal modes of pyridine was conducted. Density functional theory (DFT) implemented in the program DMol3 was employed to analyze both frequencies and excited state displacements of a Fe-porphine pyridine model complex.[52,53] The structure was geometrically optimized to a convergence of 10^{-6} Hartrees. The vibrational frequencies and eigenvectors were calculated by the finite difference method. The generalized gradient approximation (GGA) functional was used with a double-ζ quality (DNP) basis set.[54,55] The eigenvectors were displaced along a few relevant vibrational modes at 11 points (equilibrium and five displacements along the normal mode on either side of the equilibrium position). Single-point energy calculations were carried out for each displacement to generate a potential energy surface (PES) for each normal-mode analyzed.[56,57]

REPs were generated using the program *timetherm*.[40] *Timetherm* provides a calculation of the time-dependent formalism, which projects a vibrational wave function $|i\rangle$ from the ground state into an excited state whose equilibrium geometry is displaced from that of the ground state and then performs a time-dependent calculation of the overlap between $|i(t)\rangle$ and $|f\rangle$, the final vibrational state of the electronic ground state. The Fourier transformation of the overlap then gives the REP. Application of this program to the calculation of resonant Raman cross sections has been discussed elsewhere.[58,59]

RESULTS

We observed the internal modes of the pyridine by calculating the difference spectrum by spectral subtraction of d^5-pyridine from pyridine. The imidazole data did not display any enhanced internal modes. Table 1 presents the vibrational frequencies of neat aqueous pyridine.[60] Table 2 permits comparison of the vibrational frequencies in Table 1 with those of bound pyridine in the five-coordinate heme complex. In addition to the intrinsic vibrations of the pyridine ring, there is a Fe-Pyr axial stretching vibration. The substitution of d^5-pyridine for pyridine in H93G(Pyr) results in a shift of 1.6 cm^{-1} in the 207 cm^{-1} band, which has been assigned as the axial stretching vibration in previous work.[31]

Table 1. Raman Frequencies in Free Pyridine[60]

type of motion	frequency (neat)	frequency (aqueous)	symmetry	Wilson no.
in-plane ring deformation	605 cm^{-1}	618 cm^{-1}	a_1	ν_{6a}
in-plane ring deformation	652 cm^{-1}	654 cm^{-1}	b_2	ν_{6b}
trigonal breathing mode	992 cm^{-1}	1002 cm^{-1}	a_1	ν_1
ring deformation	1030 cm-1	1036 cm^{-1}	a_1	ν_{12}

Table 2. Resonance Raman Frequencies in H93G-Pyridine and H93G-d^5−Pyridine at 441.6 nm

h93g-pyridine			
type of motion	frequency	symmetry	Wilson no.
in-plane ring deformation	633 cm^{-1}	a1	ν6a
trigonal breathing mode	1007 cm^{-1}	a1	ν1
H93G d5 pyridine			
type of motion	frequency	symmetry	Wilson no.
in-plane ring deformation	610 cm^{-1}	a1	ν6a
trigonal breathing mode	979 cm^{-1}	a1	ν1

Figure 1 shows that two pyridine normal modes are also enhanced upon Soret band excitation. These modes can be identified by the isotope effect on the pyridine Raman bands from substituted d_5 isotopomer. The effect shown in Figure 2 supports the assignment of these bands as ν_1 at 1007 cm^{-1} and ν_3 at 633 cm^{-1}, based on comparison with pyridine itself. We note that the ν_1 mode of pyridine is observed at 1007 cm^{-1} on Fe metal surfaces as well.[36] The potential energy distribution in both of these modes involves coordinates that affect the nitrogen position. The trigonal ring mode, ν_1, is the analogue of the symmetric breathing mode in benzene (also ν_1), and is usually observed at 992 cm^{-1} in neat pyridine, 1002 cm^{-1} in aqueous solution, and 1008 to 1009 cm^{-1} when pyridine is adsorbed onto various metal substrates. The ring deformation known as ν_{12} is observed at 1035 cm^{-1} and usually decreases in favor of ν_1 on SERS substrates. It is at nearly the same frequency as the benzene ν_1 mode, and the potential energy consists of nearly equal contributions of all of the stretching internal coordinates. ν_3 is a symmetric ring stretching mode. The observed d^5 isotope effect on these two modes is

dx.doi.org/10.1021/jp302049p | J. Phys. Chem. B 2012, 116, 10514−10521

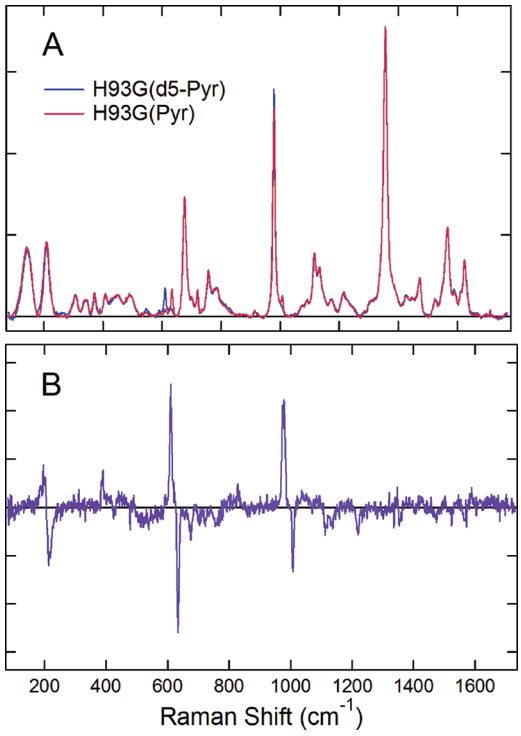

Figure 1. (A) The low-frequency Raman spectrum pf five-coordinate deoxy H93G-pyridine and H93G-d^5-pyridine was obtained at 436 nm. (B) Difference spectrum.

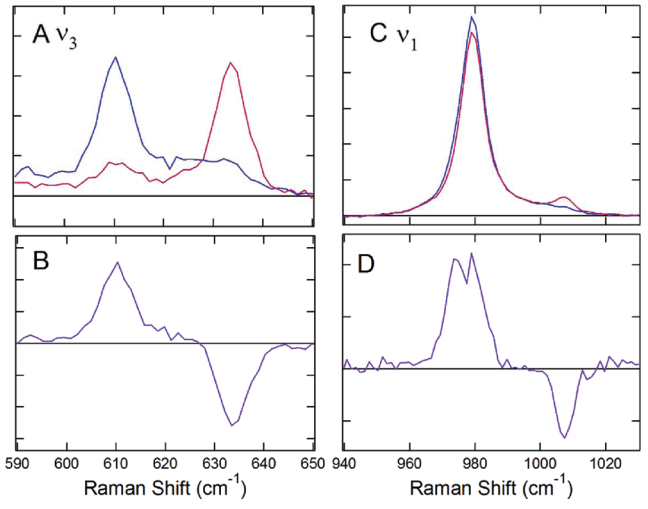

Figure 2. Expansion of the regions of the ν_1 and ν_3 modes from the spectrum shown in Figure 1. (A) The ν band is shown for H93G(Pyr) in red and H93G(d5-Pyr) in blue. (B) The difference spectrum in the same region as panel A. (C) The region of the ν_1 band is shown. The sulfate peak is also present in the spectrum. (D) The difference spectrum for the same region as panel C.

essentially identical to that presented in early studies on the normal modes of pyridine. The ν_1 mode shifts by 27 cm^{-1} to 980 cm^{-1}, and the ν_3 mode shifts by 23 cm^{-1} to 610 cm^{-1}.

The REP shown in Figure 3 gives the relative Raman intensity of the ν_3 band of the pyridine ligand. The intensity was measured at seven excitation wavelengths relative to Na_2SO_4, which was used as an internal standard. A resonance Raman spectrum obtained without the internal standard is shown for comparison in the Supporting Information as Figure

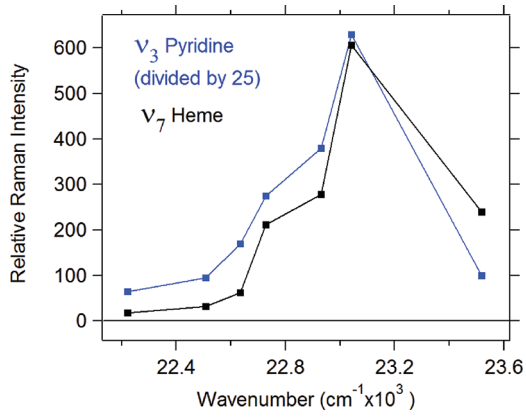

Figure 3. Experimental REP for the ν_3 mode of pyridine at 633 cm^{-1} and the ν_7 mode of heme at 675 cm^{-1}. The excitation wavelengths used were 425.2 nm, 434.0 nm, 436.1 nm, 440.0 nm, 441.8 nm, 444.3 nm, and 452.2 nm.

S1, and the corresponding difference spectrum for H93G(d^5-Pyr) − H93G(Pyr) is shown in Figure S2. The peak of the excitation is 434 nm (23,040 cm^{-1}), which corresponds roughly to the peak of the deoxy Soret band for H93G(Pyr). The REP for the pyridine ν_3 mode is shown in Figure 3 in comparison with the REP of the ν_7 mode of the heme.

Figure 4 shows the four molecular orbitals of the ground and excited states. The symmetry designations are given for the a_{1u}

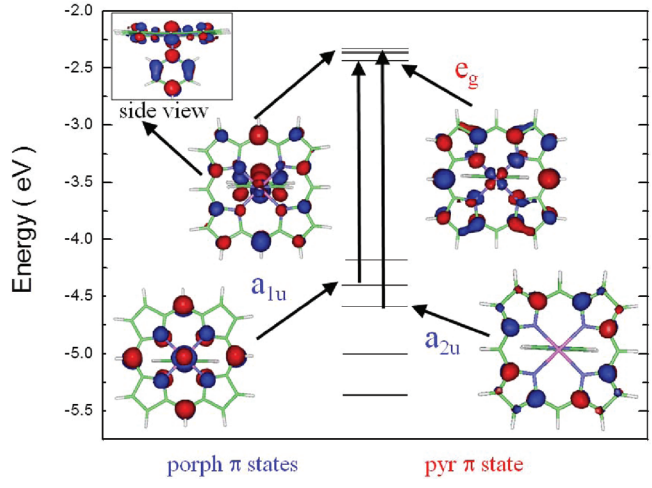

Figure 4. The energies and molecular orbitals of the relevant states involved in the $\pi-\pi^*$ transition of the heme. The calculated model is based on a five-coordinate Fe-porphine with an axial pyridine ligand (S = 2).

and a_{2u} ground state orbitals in D_{4h} symmetry. The excited state is nominally e_g and would be doubly degenerate if it were not for the axial pyridine ligand. The π orbitals of the axial pyridine mix with one of the orbitals of e_g symmetry. Figure 5A,B shows the displacement along the ν_1 and ν_3 normal modes, respectively, obtained from a vibrational frequency calculation. The calculated frequencies are 644 cm^{-1} and 1037 cm^{-1}, respectively. The displacements were used to obtain estimates for S, the electron-vibration coupling constant, which were used to calculate the REPs in panels C and D, respectively, using the program *timetherm*.[40] Calculations of a similar porphine model with an imidazole axial ligand do not show the π-type mixing

dx.doi.org/10.1021/jp302049p | J. Phys. Chem. B 2012, 116, 10514−10521

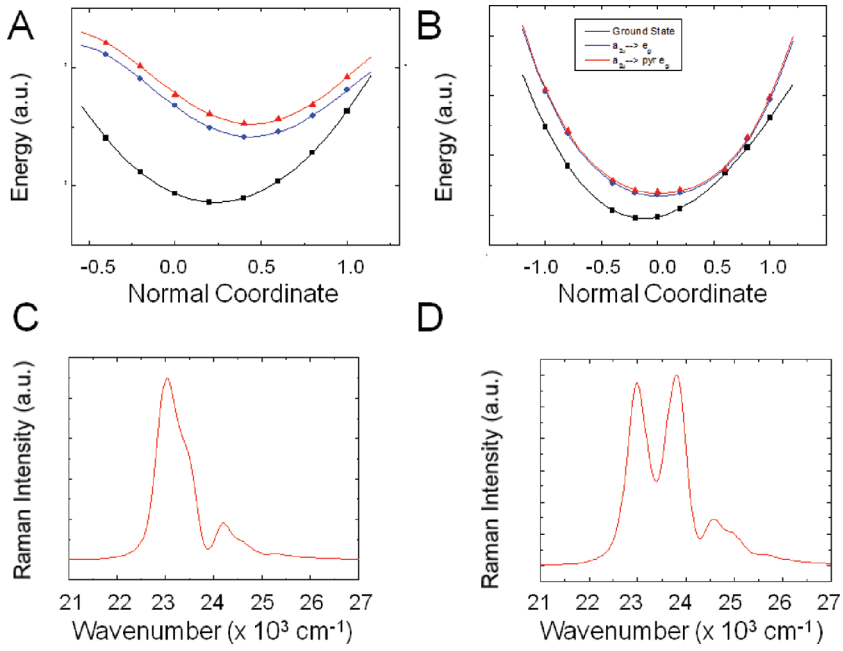

Figure 5. Calculated excited state displacements along relevant normal modes and corresponding REPs. The excited state displacements were generated by projecting along the distortions associated with the normal modes ν_1 and ν_3 identified in the text shown in panels A and B, respectively. The corresponding REPs shown in panels C and D were calculated using the time-correlator method.

for the axial ligand (see Figure S3 of the Supporting Information).

DISCUSSION

While both H93G(Im) and H93G(Pyr) exhibit isotope shifts in the region of 200−230 cm^{-1}, which have been assigned to the Fe−L out-of-plane mode,[31,39] H93G(Pyr) and substituted pyridines in the H93G mutant of SWMb show enhancement of internal vibrational modes of the pyridine.[31] The resonance enhancement of ligand out-of-plane modes is similar in both H93G(Pyr) and H93G(Im), although H93G(Pyr) derivatives have somewhat higher intensities for these modes. On the other hand, enhancement of internal ring modes such as the ν_1 and ν_3 ligand vibrational modes occurs only for H93G(Pyr) and pyridine derivatives such as 3-methyl-, 3-bromo-, and 3-fluoropyridine- ligated to the heme iron, i.e. H93G(3Me-Pyr), H93G(3Br-Pyr) and H93G(3F-Pyr).[31] We first consider the mechanistic differences that may exist between H93G(Pyr) and H93G(Im), and then proceed to a general consideration of enhancement mechanisms of axial ligands on metalloporphyrins. Finally, we will made a comparison between enhancement of axial ligands by the Soret band and enhancement by plasmon bands on metal surfaces.

The observed enhancement of axial ligand vibrations in H93G(Pyr) can be explained by a theoretical treatment that identifies the origin of the normal modes in order to establish the resonant Raman scattering mechanism. In order to distinguish between A-term[41] and B-term (Jahn−Teller and Herzberg−Teller coupling) contributions, we can examine the symmetries of the modes and their excitation profiles.[46,49] The observation of an excitation profile that follows the Soret band line shape and the excitation profile of a totally symmetric mode ν_7 of the heme suggest that the strongest mode of the axial pyridine, ν_3, is Franck−Condon active. (Figure 3). There is precedent for Franck−Condon activity for axially enhanced vibrational modes. The REP has demonstrated that the iron−histidine mode in myoglobin is enhanced predominately by an A-term scattering mechanism.[42] The enhancement of internal pyridine modes by an A-term scattering mechanism implies that there must be displacements along these normal mode coordinates in the excited state. This is confirmed by the model calculations shown in Figure 5.

We consider the nature of σ- and π-type coupling since this will further influence the interpretation of the mechanism of resonance enhancement. The Fe-His axial out-of-plane vibration has been extensively studied.[20−26] The theory for the origin of the enhancement states that the out-of-plane displacement of the Fe is crucial because it permits overlap of the d_{z2} orbital and the π-system of the heme.[28] This overlap is rigorously zero for an in-plane heme Fe, and therefore no coupling of the electronic excitation of the heme with the orbitals of the axial ligand is possible by σ-bonding interaction. Coupling with the π-system of π-acid ligands such as CO, O_2, and NO is possible for in-plane iron through intermediacy of the dπ orbitals, d_{xz} and d_{yz}.[61] Although σ-bond coupling is thought to be dominant in the case of imidazole, we will explore the hypothesis that differences in π-bond coupling may account for some of the difference in behavior of axial ligated imidazole and pyridine. In addition to these considerations, the enhancement of axial ligands in resonance Raman spectra is thought to have an important anharmonic component due to mode−mode coupling of the Fe-His mode with the Fe doming mode.[29] In previous work, we have verified this anharmonicity experimentally in a series of ligand substitutions in H93G SWMb studied as a function of temperature.[38] Studies of substituted imidazoles have shown isotope shifts of the axial Fe-L vibration; however, no other internal vibrations of the imidazole ligand have been observed in any resonance Raman spectra.[31]

The π-type resonance Raman enhancement mechanism observed in π-acid ligands of the type X−O (CO, NO, and O_2) apparently gives rise to enhancement of the internal X−O

dx.doi.org/10.1021/jp302049p | J. Phys. Chem. B 2012, 116, 10514−10521

stretching vibration, which is by far the strongest in CO. The π-acid ligands have significant interaction with the π^* excited state (e_g^*) of porphyrin rings through the dπ orbitals of the iron. Bent π-acid ligands have a π-type bonding contribution as well, but because iron is in the plane of the porphyrin in a six-coordinate Fe(II) complex, there is no Raman enhancement through these orbitals. The coupling through π-symmetry orbitals (e.g., COπ^*−dπ−e_g^* on porphyrin) is quite strong, as evidenced by the intense Raman bands that are observed. Although this mechanism can give rise to enhancement of the X−O ligand stretching in some cases, the coupling of π-acid ligands appears to be qualitatively different from that of imidazole, since it involves extensive interaction of the π-system on the metal with the π^* orbital of the bound diatomic ligand. By contrast, the bonding of imidazole appears to be dominated by σ-type interactions involving an orbital that is essentially a nitrogen lone pair (called N_ε) and the d_{z2} orbital of the iron. The so-called lone pair orbital of imidazole has been identified as 15a″ from ab initio calculations. The question arises whether pyridine can involve a greater extent of π-bonding interaction than imidazole or, alternatively, whether the energy of the nitrogen lone pair in pyridine may play a decisive role. These two factors may also act in concert to explain the observed enhancement of the ν_1 and ν_3 modes of pyridine in H93G(Pyr).

The origin of the mixing of the e_g excited state with pyridine orbitals, and not with imidazole π-orbitals can be understood based on the properties of the molecules themselves. The lowest electronic transitions in pyridine are nearly degenerate n−π^* and π−π^* transitions (at ca. 275 nm in solution). By contrast, the lowest electronic transition of imidazole is at 207 nm in solution and has been identified as a π−π^* transition. The n−π^* transition in imidazole is calculated to be at significantly higher energy. A comparison of the ionization potentials for the nonbonding n-type orbital (15a′ in imidazole and Xa1 in pyridine) shows that these are nearly the same. However, since the n−π^* transition in imidazole is at 8 eV while that in pyridine is at 4.5 eV, the axial-ligand π^* orbital is significantly closer in energy to the dπ of the iron for pyridine than for imidazole. Thus, the coincidence of the orbital energies of a σ- and π-type bonding (i.e., those for n−π * and π−π^*) may explain both the similar resonance enhancement of the Fe−L out-of-plane modes for pyridine and imidazole as due to similar mixing of the ground state N_ε with the iron d_{z2} orbital, while at the same time allowing a difference in the coupling of the π systems due to the large energy difference in the π^* orbitals that gives rise to the coupling of ring modes uniquely in pyridine.

An alternative explanation for the difference between imidazole and pyridine could be the coincidence of a CT transition with the Soret band. Figure 4 shows that one of the two excited states has significant π-bonding character. However, in this case we do not see evidence in the calculations for a metal-to-ligand charge transfer (MLCT), but rather the π-bonding mechanism for electronic excitation, which leads to a change in the electron density on the pyridine, arises mostly from coupling to the π−π^* or Soret band transition. This is essentially a delocalization of electron density from the e_g^* state to the π system of the ligand. While we cannot rule out a role for a buried CT transition, the experimental result and calculations suggest that the dominant contribution to Raman enhancement in H93G(Pyr) arises from resonant coupling to the Soret band.

On the basis of the foregoing considerations, coupling of the pyridine ring to the heme via the π-system of pyridine is consistent with Raman enhancement of the trigonal ring breathing mode (ν_1) and the symmetric ring stretch (ν_3) as axial intramolecular modes. The enhancement arises since the electron density shifts on the pyridine ring involve a reduction of electron density in the n-type orbital (by mixing with d_{z2} and the ground state a_{2u} orbital) and an increase in electron density in the π^* orbital by mixing with the dπ and porphyrin e_g^* orbitals. The enhancement of modes of pyridine by excitation of the orthogonal porphyrin ring compared to dilutions of pyridine in aqueous solution provide an estimate of approximately 2000 for the enhancement factor for the ν_3 mode as a result of bonding to the heme Fe. It is noteworthy that the ν_1 and ν_3 modes are also among those modes that show the greatest enhancement when pyridine is bound to Ag surfaces.[6,14,47] We have recently considered a model for such resonant enhancement in Ag clusters based on both DFT calculations and absorption spectra of pyridine-Ag nanoparticle model systems and found that it is consistent as an explanation for the observations of large enhancement of pyridine on Ag.[1] The experiments and calculations presented here further lend support to the hypothesis that resonant enhancement of axial modes is potentially a major contribution to SERS.[1] If we consider porphyrin as the kind of surface to which pyridine is bound, then we can speak of surface enhancement of pyridine on heme by analogy with SERS on metal surfaces as determined previously in comparisons of a range of transition metals.[36,62] Resonance Raman can easily lead to enhancement by factors of greater than 10^3 for ligands bound to a metal center. Given that the Ag-pyridine system has typical enhancement factors of $\sim 10^6$,[63] one can conclude that the resonance Raman effect could be as large as the electromagnetic effect in the most studied of all SERS systems, pyridine on a Ag surface. On the basis of these considerations, we propose that Raman resonance is a more important contribution to SERS than has been considered in previous work.

The present study can be placed in the context of the study of the mechanism of SERS, which remains a subject of debate more than 35 years after the first observation of an effect of roughened Ag on the Raman scattering of adsorbed pyridine.[9] The observation of large Raman scattering signals from pyridine on Ag surfaces and colloids started a field of investigation that, in recent decades, has led to reports of single-molecule Raman scattering.[64,65] While the early studies were based on statistical arguments, independent confirmation of single-molecule surface enhanced resonant Raman scattering (SERRS) has recently been provided for one specific case of Rhodamine dye on Ag.[66,67] The large number of studies of Rhodamine on Ag using conditions under which the Rhodamine itself is resonantly enhanced underscores the importance of resonance enhancement in the overall effect of SERRS[68] and suggests that similar considerations should be applied to the plasmon band in SERS itself, as we have argued based on recent DFT calculations of pyridine on Ag clusters.[1]

The magnitude of the local field enhancement estimated by various calculations varies greatly and can be anywhere in the range of 10^3−10^{15}, depending on geometry and resonance conditions.[69−72] All investigators agree that both a chemical and electromagnetic effect are required to explain the large enhancements necessary for single-molecule effects. The fact that pyridine has a strong connection to Ag surfaces is evident from the fact that it has a Ag−N stretching frequency of 239

cm^{-1},[63,73] which is even higher than the 209 cm^{-1} frequency for the Fe−N stretch of pyridine in H93G(Pyr).[31] This strong connection between the molecule and the Ag has led some to suggest that the chemical mechanism is mostly a CT effect between the metal and adsorbate.[3] While CT bands certainly can play a role, the present work suggests that a much more general effect, namely, excited state displacement due to coupling of a ligand to a molecular system with a large absorption band, is also a possible origin for SERS. Here we propose the analogy of the Soret band on heme and the plasmon band on a Ag particle or surface and that the effect of each on a bound pyridine adsorbate could be similar due to coupling of metal d orbitals to the π-system of the pyridine adsorbate.

Although the magnitude of the chemical effect is often considered to be minor,[74] our previous work has suggested that, on the contrary, there is an intrinsic limitation to the electromagnetic effect due to bandwidth considerations that have not been considered in previous work.[75] The SERS bandwidth presents an important limitation on the magnitude of the electromagnetic effect, which may be much smaller than many have estimated due to the fact that the energy stored in the conductor can only originate from the exciting laser, and this can only enhance within a narrow range near the peak of the plasmon band.[75] The electromagnetic contribution arises from the local field effect due to the curvature of the conducting substrate.[76] However, since electromagnetic enhancement requires excitation into the plasmon resonance band, in order to obtain large local fields, this effect has an intrinsic spectral bandwidth, which is quite narrow (<1 nm) for the conditions that permit an enhancement factor of $\sim 10^6$ on a single Ag particle.[75] There is increasing awareness that resonance Raman effects can rival the electromagnetic component in SERRS,[68,77] which suggests that resonance effects of the plasmon band itself could be important in SERS. The present work suggests that molecular interactions with the metal surface can give rise to significantly more important effects than the proponents of the electromagnetic theory have suggested. The support for strong interaction between molecules and surfaces can be seen in the effects on molecular spectra of adsorbed molecules.[78,79] Molecular spectra are strongly affected following adsorption, which indicates that in many cases molecules interact strongly with the metal leading to the possibility of enhancement by excited state nuclear displacement, a requirement for Franck−Condon or A-term resonance Raman scattering. On the basis of these considerations, we suggest that plasmonic effects may consist of considerable contributions from resonant Raman scattering of adsorbed molecules that couple to the metal in a manner analogous to the coupling of pyridine on heme as shown in the present study.

■ ASSOCIATED CONTENT

Supporting Information

Resonance Raman spectra without an Na_2SO_4 internal standard, REPs as a function of wavelength, and molecular orbitals from DFT calculations of a porphine model complex with axial histidine are shown. This material is available free of charge via the Internet at http://pubs.acs.org.

■ AUTHOR INFORMATION

Notes

The authors declare no competing financial interest.

■ ACKNOWLEDGMENTS

The authors would like to thank Drs. Andrew Shreve and Rich Mathies for making the program *timetherm* available for the conduct of this work. We thank Dr. Steven G. Boxer for the *E. coli* strain with a pUC-19 plasmid containing the H93G Sperm whale myoglobin gene. S.F. gratefully acknowledges support from National Science Foundation grant number CHE1112017.

■ REFERENCES

(1) Gaff, J. F.; Franzen, S. *Chem. Phys.* **2012**, *397*, 34.
(2) Arenas, J. F.; Tocon, I. L.; Woolley, M. S.; Otero, J. C.; Marcos, J. I. *J. Raman Spectrosc.* **1998**, *29*, 673.
(3) Birke, R. L.; Znamenskiy, V.; Lombardi, J. R. *J. Chem. Phys.* **2010**, 132.
(4) Cao, P. G.; Gu, R. A.; Ren, B.; Tian, Z. Q. *Chem. Phys. Lett.* **2002**, *366*, 440.
(5) Chavez-Gil, T. E.; de Faria, D. L. A.; Toma, H. E. *Vibrational Spectroscopy* **1998**, *16*, 89.
(6) Chen, C. Y.; Burstein, E.; Lundquist, S. *Solid State Commun.* **1979**, *32*, 63.
(7) Creighton, J. A.; Albrecht, M. G.; Hester, R. E.; Matthew, J. A. D. *Chem. Phys. Lett.* **1978**, *55*, 55.
(8) Demuth, J. E.; Christmann, K.; Sanda, P. N. *Chem. Phys. Lett.* **1980**, *76*, 201.
(9) Fleischmann, M.; Hendra, P. J.; McQuillan, A. J. *Chem. Phys. Lett.* **1974**, *26*, 163.
(10) Jensen, L.; Zhao, L. L.; Schatz, G. C. *J. Phys. Chem. C* **2007**, *111*, 4756.
(11) Lee, M. T.; Wu, D. Y.; Tian, Z. Q.; Lin, S. H. *J. Chem. Phys.* **2005**, 122.
(12) Lever, A. B. P.; Ramaswam., Bs. *Can. J. Chem.* **1973**, *51*, 1582.
(13) Lombardi, J. R.; Birke, R. L. *J. Phys. Chem. C* **2010**, *114*, 7812.
(14) Loo, B. H.; Furtak, T. E. *Chem. Phys. Lett.* **1980**, *71*, 68.
(15) Mizutani, G.; Ushioda, S. *J. Chem. Phys.* **1989**, *91*, 598.
(16) Saito, Y.; Schlapfe., Cw; Cordes, M.; Nakamoto, K. *Appl. Spectrosc.* **1973**, *27*, 213.
(17) Vanduyne, R. P.; Haushalter, J. P. *J. Phys. Chem.* **1983**, *87*, 2999.
(18) Wright, P. G.; Stein, P.; Burke, J. M.; Spiro, T. G. *J. Am. Chem. Soc.* **1979**, *101*, 3531.
(19) Zhao, L. L.; Jensen, L.; Schatz, G. C. *J. Am. Chem. Soc.* **2006**, *128*, 2911.
(20) Argade, P. V.; Sassaroli, M.; Rousseau, D. L.; Inubushi, T.; Ikeda-Saito, M.; Lapidot, A. *J. Am. Chem. Soc.* **1984**, *106*, 6593.
(21) Friedman, J. M.; Scott, T. W.; Stepnowski, R. A.; Ikeda-Saito, M.; Yonetani, T. *J. Biol. Chem.* **1983**, *258*, 10564.
(22) Kitagawa, T.; Kyogoku, Y.; Iizuka, T.; Saito, M. I. *J. Am. Chem. Soc.* **1976**, *98*, 5169.
(23) Kitagawa, T.; Nagai, K.; Tsubaki, M. *FEBS Lett.* **1979**, *104*, 376.
(24) Desbois, A.; Lutz, M.; Banerjee, R. *Biochemistry* **1979**, *18*, 1510.
(25) Spiro, T. G.; Smulevich, G.; Su, C. *Biochemistry* **1990**, *29*, 4497.
(26) Wells, A. V.; Sage, T. J.; Morikis, D.; Champion, P. M.; Chiu, M. L.; Sligar, S. G. *J. Am. Chem. Soc.* **1991**, *113*, 9655.
(27) Wang, J. L.; Takahashi, S.; Rousseau, D. L. *Proc. Natl. Acad. Sci. U.S.A.* **1995**, *92*, 9402.
(28) Stavrov, S. S. *Biophys. J.* **1993**, *65*, 1942.
(29) Rosenfeld, Y. B.; Stavrov, S. S. *Chem. Phys. Lett.* **1994**, *229*, 457.
(30) Decatur, S. M.; Franzen, S.; DePillis, G. D.; Dyer, R. B.; Woodruff, W. H.; Boxer, S. G. *Biochemistry* **1996**, *35*, 4939.
(31) Franzen, S.; Boxer, S. G.; Dyer, R. B.; Woodruff, W. H. *J. Phys. Chem. B* **2000**, *104*, 10359.
(32) Barrick, D. *Biochemistry* **1994**, *33*, 6546.
(33) Thomas, M. R.; Brown, D.; Franzen, S.; Boxer, S. G. *Biochemistry* **2001**, *40*, 15047.
(34) Pond, A. E.; Roach, M. P.; Sono, M.; Rux, A. H.; Franzen, S.; Hu, R.; Thomas, M. R.; Wilks, A.; Dou, Y.; Ikeda-Saito, M.; de Montelano, P. R. O.; Woodruff, W. H.; Boxer, S. G.; Dawson, J. H. *Biochemistry* **1999**, *38*, 7601.

(35) DePillis, G.; Decatur, S. M.; Barrick, D.; Boxer, S. G. *J. Am. Chem. Soc.* **1994**, *116*, 6981.
(36) Andrade, G. F. S.; Temperini, M. L. A. *J. Raman Spectrosc.* **2009**, *40*, 989.
(37) Le Moigne, C.; Picaud, T.; Boussac, A.; Loock, B.; Momenteau, M.; Desbois, A. *Inorg. Chem.* **2003**, *42*, 6081.
(38) Franzen, S.; Fritsch, K.; Brewer, S. H. *J. Phys. Chem. B* **2002**, *106*, 11641.
(39) Franzen, S.; Peterson, E. S.; Brown, D.; Friedman, J. M.; Thomas, M. R.; Boxer, S. G. *Eur. J. Biochem.* **2002**, *269*, 4879.
(40) Shreve, A. P.; Mathies, R. A. *J. Phys. Chem.* **1995**, *99*, 7285.
(41) Albrecht, A. C. *J. Chem. Phys.* **1961**, *34*, 1476.
(42) Bangcharoenpaurpong, O.; Schomaker, K. T.; Champion, P. M. *J. Am. Chem. Soc.* **1984**, *106*, 5688.
(43) Abe, M.; Kitagawa, T.; Kyogoku, Y. *J. Chem. Phys.* **1978**, *69*, 4526.
(44) Li, X.-Y.; Czernuszewicz, R. S.; Kincaid, J. R.; Stein, P.; Spiro, T. G. *J. Phys. Chem.* **1990**, *94*, 47.
(45) Li, X.-Y.; Czernuszewicz, R. S.; Kincaid, J. R.; Su, Y. O.; Spiro, T. G. *J. Phys. Chem.* **1990**, *94*, 31.
(46) Franzen, S.; Wallace-Williams, S. E.; Shreve, A. P. *J. Am. Chem. Soc.* **2002**, *124*, 7146.
(47) Vivoni, A.; Birke, R. L.; Foucault, R.; Lombardi, J. R. *J. Phys. Chem. B* **2003**, *107*, 5547.
(48) Lombardi, J. R.; Burke, J. M. *Acc. Chem. Res.* **2009**, *42*, 734.
(49) Shelnutt, J. A. *J. Chem. Phys.* **1981**, *74*, 6644.
(50) Potapkina, E. V.; Denisova, A. S.; Myund, L. A.; Makarov, A. A.; Dem'yanchuk, E. M. *J. Mol. Struct.* **2011**, *996*, 128.
(51) Franzen, S.; Bailey, J.; Dyer, R. B.; Woodruff, W. H.; Hu, R. B.; Thomas, M. R.; Boxer, S. G. *Biochemistry* **2001**, *40*, 5299.
(52) Delley, B. *J. Chem. Phys.* **1990**, *92*, 508.
(53) Delley, B. *J. Chem. Phys.* **2000**, *113*, 7756.
(54) Perdew, J. P.; Burke, K.; Ernzerhof, M. *Phys. Rev. Lett.* **1996**, *77*, 3865.
(55) Perdew, J. P.; Wang, Y. *Phys. Rev. B* **1992**, *45*, 13244.
(56) Lappi, S. E.; Collier, W.; Franzen, S. *J. Phys. Chem. A* **2002**, *106*, 11446.
(57) Lappi, S. E.; Franzen, S. *Spectrochim. Acta A* **2004**, *60*, 357.
(58) Gaff, J. F.; Franzen, S. *J. Phys. Chem. A* **2009**, *113*, 5414.
(59) Gaff, J. F.; Franzen, S.; Delley, B. *J. Phys. Chem. A* **2010**, *114*, 11681.
(60) Creighton, J. A.; Alvarez, M. S.; Weitz, D. A.; Garoff, S.; Kim, M. W. *J. Phys. Chem.* **1983**, *87*, 4793.
(61) Ray, G. B.; Li, X.-Y.; Ibers, J. A.; Sessler, J. L.; Spiro, T. G. *J. Am. Chem. Soc.* **1994**, *116*, 162.
(62) Zuo, C.; Jagodzinski, P. W. *J. Phys. Chem. B* **2005**, *109*, 1788.
(63) Jeanmaire, D. L.; Vanduyne, R. P. *J. Electroanal. Chem.* **1977**, *84*, 1.
(64) Kneipp, K.; Wang, Y.; Kneipp, H.; Perelman, L. T.; Itzkan, I.; Dasari, R.; Feld, M. S. *Phys. Rev. Lett.* **1997**, *78*, 1667.
(65) Nie, S. M.; Emery, S. R. *Science* **1997**, *275*, 1102.
(66) Hildebrandt, P.; Stockburger, M. *J. Phys. Chem.* **1984**, *88*, 5935.
(67) Dieringer, J. A.; Lettan, R. B., II; Scheidt, K. A.; Van Duyne, R. P. *J. Am. Chem. Soc.* **2007**, *129*, 16249.
(68) Le Ru, E. C.; Blackie, E.; Meyer, M.; Etchegoin, P. G. *J. Phys. Chem. C* **2007**, *111*, 13794.
(69) Jiang, J.; Bosnick, K.; Maillard, M.; Brus, L. *J. Phys. Chem. B* **2003**, *107*, 9964.
(70) Kneipp, K.; Kneipp, H.; Deinum, G.; Itzkan, I.; Dasari, R. R.; Feld, M. S. *Appl. Spectrosc.* **1998**, *52*, 175.
(71) Michaels, A. M.; Nirmal, M.; Brus, L. E. *J. Am. Chem. Soc.* **1999**, *121*, 9932.
(72) Xu, H. X.; Bjerneld, E. J.; Kall, M.; Borjesson, L. *Phys. Rev. Lett.* **1999**, *83*, 4357.
(73) Lombardi, J. R.; Knight, E. A. S.; Birke, R. L. *Chem. Phys. Lett.* **1981**, *79*, 214.
(74) Moskovits, M. *Rev. Mod. Phys.* **1985**, *57*, 783.
(75) Franzen, S. *J. Phys. Chem. C* **2009**, *113*, 5912.
(76) Gersten, J. I.; Nitzan, A. *J. Chem. Phys.* **1980**, *73*, 3023.
(77) Haes, A. J.; Duyne, R. P. V. *Anal. Bioanal. Chem.* **2004**, *379*, 920.
(78) Franzen, S.; Folmer, J. C. W.; Glomm, W. R.; O'Neal, R. *J. Phys. Chem. A* **2002**, *106*, 6533.
(79) McLaughlin, C.; Graham, D.; Smith, W. E. *J. Phys. Chem. B* **2002**, *106*, 5408.